Electrical Power and Energy Systems 54 (2014) 399–407

Contents lists available at ScienceDirect

Electrical Power and Energy Systems

journal homepage: www.elsevier.com/locate/ijepes

Virtual active filters for HVDC networks using V2G technology

F.R. Islam *, H.R. Pota

School of Engineering & Information Technology, The University of New South Wales, Canberra, ACT 2600, Australia

ARTICLE INFO

Article history:
Received 23 July 2012
Received in revised form 9 July 2013
Accepted 23 July 2013

Keywords:
Power system
HVDC
Active filter
PHEV
V2G

ABSTRACT

Active and passive filters are essential to maintain the power quality of a HVDC link. In this paper the Vehicle to Grid (V2G) technology is used to design a virtual active filter based on instantaneous power theory (p–q theory). The potential of a low-cost solution that utilizes the reactive power and filtering capabilities of plug-in vehicles parked in charging stations is investigated. Simulations are performed for the CIGRE benchmark HVDC network to demonstrate that the proposed virtual active filter improves the power quality maintaining the IEEE Std 519-1992.

1. Introduction

In recent years, there have been significant advances in battery and hybrid-electric power technologies which coupled with energy security requirements, financial and, environmental concerns and the rising costs of petroleum, make plug in hybrid electrical vehicles (PHEVs) a strong alternative to conventional vehicle [1,2]. It is envisioned that most vehicles manufactured in the future will have a plug-in option for recharging their batteries and, by the year 2030, PHEV penetration will be nearly 25% [3]. PHEVs can be charged from various locations, such as a house-hold's electrical connection, a charging station as well as from the car park during the day. Various researchers have come forward to find out the optimal placements of PHEV's charging station and parking [4–8]. With PHEVs come the opportunities to design bidirectional charger as active filter for HVDC networks.

V2G operation can be explained in a number of ways as PHEVs can serve grids as regulators, spinning reserves, storage for renewable energy sources and reactive power compensators to provide improvement in power quality.

Ideas for using PHEV charging station as a spinning reserve [9], for load leveling [10], and external storage for renewable energy [11], have been studied, and a PHEV for improving the quality of wind power has been reported in [12]. Another study has demonstrated that a PHEV battery can serve as a STATCOM [13]. Dynamic voltage restorers (DVRs) have been designed using PHEV in [14] and virtual UPFC model is developed in [15]. Effective pricing models of the buying and selling of electricity from a PHEV using variable price curves are reported in [16,17].

The use of an active filter in an HVDC network was first demonstrated in 1993 at Skagerrak3 HVDC Intertie and then at Baltic Cable HVDC Link in 1994 and Chandrapur-Padghe HVDC Power transmission in 1998 [18]. The main aim of an active filter is to reduce harmonics and to compensate reactive power at the same time.

To reduce risk in an integrated vehicle health maintenance system a fuzzy multi-sensor data fusion Kalman filter model is used in [19] and the filtering capability of a single vehicle has been utilized in photovoltaic and wind power systems in [20,21] respectively. However previous studies have not dealt with the possibility of a fleet of such vehicles being parked in a charging station or the usefulness in bulk amounts in an HVDC transmission network. This paper presents a way of analyzing the filtering and reactive power transaction capabilities of the V2G mode of operation for PHEVs.

A simple structure of an HVDC network can be described as a transmission system with a set of rectifier and inverter for interfacing a DC line with an AC network. A future smart grid consisting of an HVDC system has been anticipated since the late eighties and early nineties [22]. However its drawback has been the high cost of power electronics based converters and inverters and their control. For the last few years, a great deal of effort has been made to reduce these costs and improve HVDC technology [23–27]. As a result, American, several European countries and some Asian countries and Australia currently have HVDC power networks. An HVDC network has some important niche applications compared with other systems or devices. The main application of HVDC

* Corresponding author. Tel.: +61 02 6268 8924; fax: +61 02 6268 8581.
E-mail addresses: fr.islam81@yahoo.com.au, F.M.Islam@student.adfa.edu.au (F.R. Islam).

0142-0615/$ - see front matter © 2013 Elsevier Ltd. All rights reserved.
http://dx.doi.org/10.1016/j.ijepes.2013.07.028

network is to transmit electric power over long distances and submarine connections.

Harmonics are created from the nonlinear operation of HVDC converters on both the AC and DC side of the link which can be identified as characteristic or no characteristic. Although under ideal conditions characteristic harmonics are related to the pulse number of the converter, in fact, in a real system these ideal conditions are not achievable. Therefore, no characteristic harmonics are usually present in an HVDC network.

As the harmonics in power system create power loss and can sometimes cause operational failures of electronic components, their reduction is essential for installed equipment [28–30]. In an HVDC network, capacitor based active filters which are a combination of electronics converters, capacitors and switching controller, are used to reduce harmonics [18]. The most expensive components for the constitution of FACTS or filter devices are their capacitors [31]. In this paper, the capacitors are replaced by a PHEV parking station and the PHEV's bidirectional charger is used as the converter. The p–q theory [28] is used to design a controller and the possibility of employing PHEVs as a virtual active filter in an HVDC network to achieve a low cost filter solution is investigated, with the following two case studies introduced to verify its performance:

- Case1: virtual active filter for the rectifier side of the HVDC link.
- Case2: virtual active filter for both the rectifier and inverter sides of the HVDC link.

The rest of the paper is organized as follows: Section 2 describes the HVDC test system; PHEV battery modeling and network interfacing are presented in Section 3; Section 4 presents the controller design; and Section 5 contains the simulation results. Finally, Section 6 provides brief remarks and suggestions for future work.

2. HVDC test system

The CIGRE benchmark model [32–34] is taken as the base system for addressing harmonics problems which exhibits complex operational characteristics. The system shown in Fig. 1 is a 12-pulse 500 kV HVDC link rated at 1000 MW in which the T-section represents the DC-line. The control model at the rectifier is constant current control and at the inverter it is constant extinction angle (γ) control. The converters (rectifier and inverter) are modeled using six-pulse Graetz bridge block. The block consists of an internal phase locked oscillator (PLO), firing angle measurements and firing and valve blocking controls. Each thyristor has a built-in RC snubber circuit. Both inverter and converter sides have similar model of the converter's transformer. A combination of a three-phase two winding transformer, one with a grounded Wye–Wye connection and the other a grounded Wye–Delta connection are used. Saturation characteristics are modeled with a tap setting arrangement and smoothing reactors are inserted on both sides with an equivalent T-network to model the DC line. Three phase AC voltage sources are used to represent the supply voltages on both converter sides and tuned filters and reactive power supports are provided at both the rectifier and the inverter AC sides, as shown in Fig. 1.

The aim of this research is to replace the tuned filter and reactive power support from both the converter's sides using PHEV as a virtual active filter to obtain a low cost filter and to demonstrate that the HVDC terminal is a suitable connection place for PHEV parks, as shown in Figs. 2 and 3.

3. PHEV battery modeling and network interfacing

PHEVs are able to compensate reactive power to utility grid, as reported in [13]. In this work, they are considered as bidirectional converters connected dynamic batteries [35]. The bidirectional converters are designed with a rated current 70 A and the PHEV's power capabilities are within the range of ±20 kW active and ±20 kV A reactive. Virtual filters are considered for ±20 MW of power transaction in the grid that is a park with around 1000 vehicles which is quite a reasonable assumption for city car parks. Here the "+" sign indicates that the PHEV is in the V2G mode of operation and "−" that it is in the G2 V mode. The P–Q capability of a realistic PHEV battery varies ±138 kW and between ±126 kV A as shown in Fig 4 [13,36].

A dynamic model of a rechargeable battery [37], the operation of which depends on the electrolyte temperature (θ), state of charge (SOC) and i_m is an integral part of the total current (i_{dc}) as shown in the battery equivalent network in Fig. 5 is used. Another part of the total current passes through the parasitic branch the reaction of which is a continuous process, but not participating in the main reaction. The voltage across this parasitic branch is nearly equal to the voltage at the main reaction branch and the power dissipated in real part of impedances Z_m and Z_p is converted into heat. The impedance of the main reaction branch increases with charge and, as a result, the terminal voltage of the parasitic branch rises as does the current I_p. At the full state of battery charge, this impedance approaches infinity [37–39]. This battery model can be represented as an RLC network as shown in Fig. 6, in which the number of RLC blocks, can be kept limited as the specific speed of evolution of electric quantities change very rapidly for a PHEV [37].

The third-order battery dynamic model is designed considering the current, electrolyte temperature and SOC and its dynamic equations are [37–40]:

$$\dot{q}_e = \frac{i_{dc}}{T_s} \tag{1}$$

$$\dot{i}_m = \frac{(i_{dc} - i_m)}{T_m} \tag{2}$$

$$\dot{\theta} = -\frac{1}{C_\theta}\left[P_s - \frac{\theta - \theta_a}{R_\theta}\right] \tag{3}$$

$$V_{dc} = E_m - V_p(q_e, i_m) + V_e e^{-\beta_e q_e} - R_0 i_{dc} \tag{4}$$

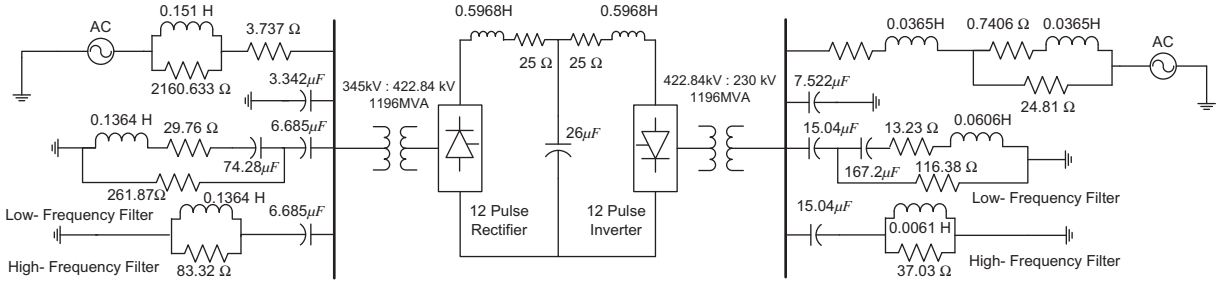

Fig. 1. Single-line diagram of CIGRE benchmark HVDC system [16].

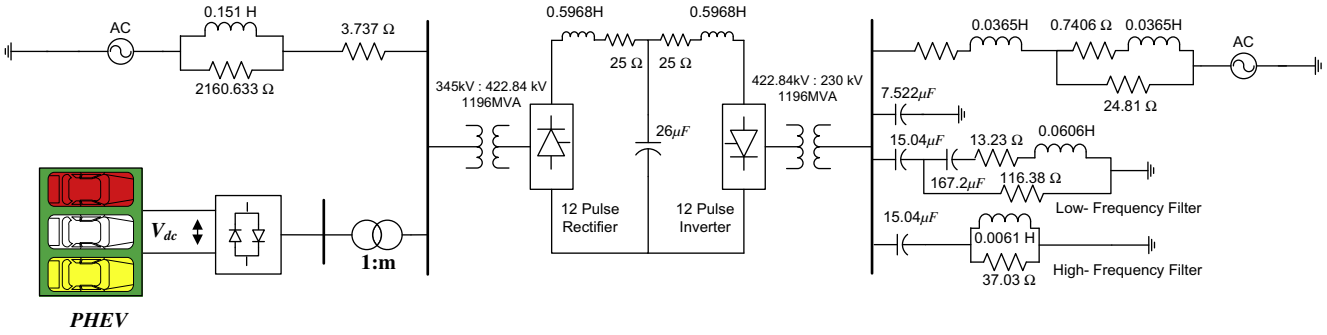

Fig. 2. Modified CIGRE benchmark HVDC system with virtual filter on rectifier side.

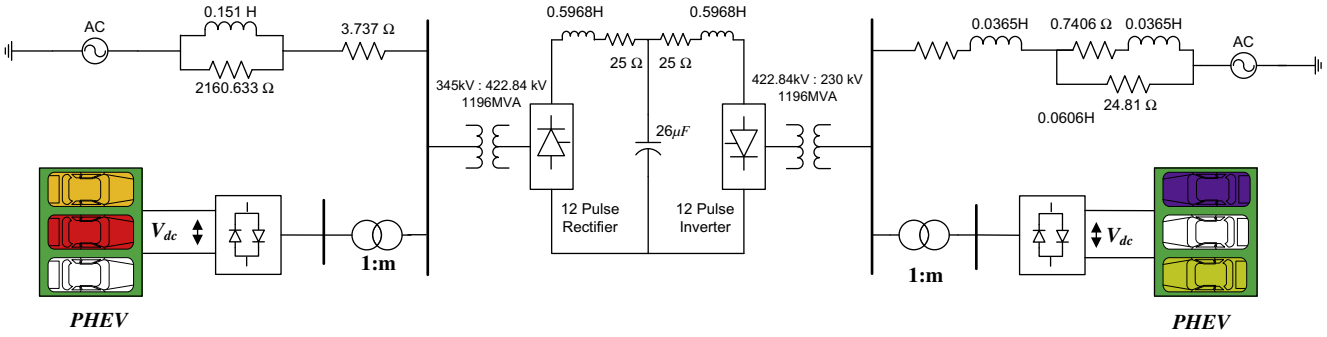

Fig. 3. Modified CIGRE benchmark HVDC system with virtual filter on both sides.

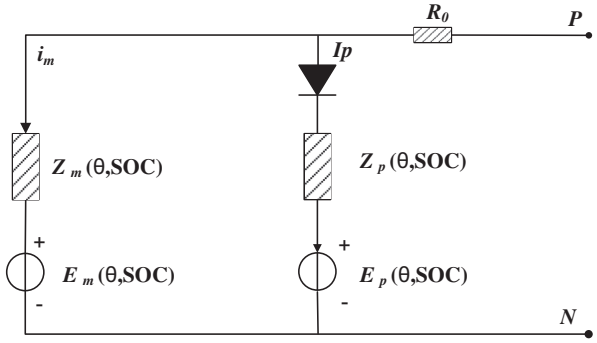

Fig. 4. Battery equivalent network with parasitic branch.

where V_e represents the hysteresis phenomenon for the battery during charge and discharge cycles. The voltage (V_{dc}) increases when the battery is charging and decreases when it's discharging. The polarization voltage (V_p) depends on the sign of i_m as

$$V_p(q_e, i_m) = \begin{cases} \frac{R_p i_m + K_p q_e}{SOC} & \text{if } i_m < 0 \text{ (discharge)} \\ \frac{R_p i_m}{q_e + 0.1} + \frac{K_p q_e}{SOC} & \text{if } i_m < 0 \text{ (charge)} \end{cases}$$

The equations for E_m, R_0, R_1, and R_2 are

$$E_m = E_{m0} - K_e(273 + \theta)(1 - SOC) \quad (5)$$

$$R_0 = R_{00}[1 + A_0(1 - SOC)] \quad (6)$$

$$R_1 = -R_{10}\ln(\text{DOC}) \quad (7)$$

$$R_2 = R_{20}\frac{\exp[A_{21}(1 - SOC)]}{1 + \exp(A_{22} I_m / I^*)} \quad (8)$$

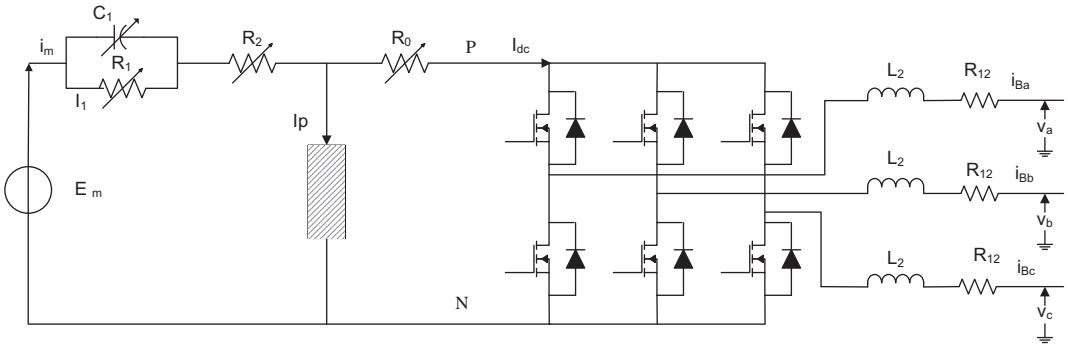

Fig. 5. PHEVs connection with power system network.

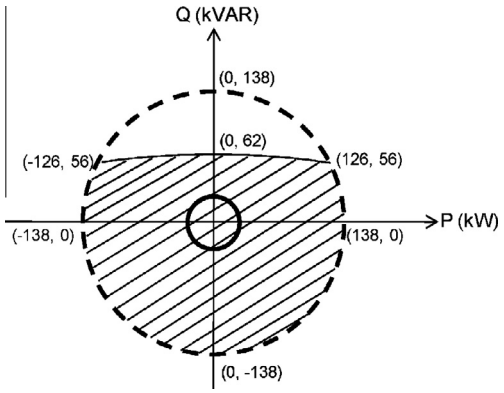

Fig. 6. PQ capability of a vehicle battery [23].

The SOC and depth of charge (DOC) can be expressed as

$$SOC = \frac{Q_n - Q_e}{Q_n} = 1 - q_e \tag{9}$$

$$\mathrm{DOC} = 1 - \frac{Q_e}{C(I_{avg}, \theta)} \tag{10}$$

where C_θ and P_s are the battery's thermal capacity and power respectively, R_0 is the thermal resistance and R_p is the polarization resistance, θ_a is the ambient temperature, I^* is the reference current (a good choice of I^* is a current that flows in the battery for typical use), x_r is the Thevenin equivalent reactance, β_e is the exponential capacity coefficient, Q_e is the extracted capacity in Ah, Q_n is the rated battery capacity in Ah and E_m, K_e, K_p, A_0, A_{21} and A_{22} are constant for a particular battery. The details battery parameters are available in [13,14], and few important parameters are shown in Appendix A.

The behavior of the parasitic branch is strongly nonlinear and its current is given as

$$I_p = V_p G_p \exp\left(\frac{V_p}{V_{p0}} + A_p\left(1 - \frac{\theta}{\theta_f}\right)\right) \tag{11}$$

The heat produce by the parasitic reaction can be calculated by means of the Joule law, as given in the following equation

$$P_s = R_p I_p^2 \tag{12}$$

where θ_f is the electrolytic freezing temperature and V_{po}, G_p, and A_p are constants.

4. Controller design

4.1. General control principle

The target of the controller design is to control the switching of the PHEV's converter in such way that the PHEV Park can be used as a filter and to compensate the reactive power consumed by the HVDC link.

The virtual active filter controller is divided into three functional control blocks:

1. Instantaneous-power calculation,
2. Power-compensating,
3. DC-voltage regulation and current control.

The instantaneous power of the nonlinear load is calculated by the first block while the second controls the behavior of the virtual active filter which determines the parts of the real power and imaginary power of the nonlinear load that need to be compensated. The third block represents the DC voltage regulator which calculates an extra amount of real power (P_L) to maintain the voltage around a fixed reference value. P_L is added to the compensating real power and passed to the current-reference calculation block together with the compensating imaginary power. Then this block determines the instantaneous compensating current references from the compensating power and voltages as shown in Fig. 7.

4.2. Instantaneous power calculation

An instantaneous power calculation method is presented in [41] to design active power filters for EV charging, where, instantaneous values are transformed into a *DQ*-frame converting a nonlinear instantaneous power relationship into a linear one, and a detailed closed-loop model is developed for stability analysis using the *DQ* theory. In general *DQ* theory is the projection of the phase quantities onto a rotating reference frame, on the other hand *PQ* theory can be thought of as the projection of the phase quantities onto a stationary two-axis reference frame [28]. *PQ* Theory has become a very attractive tool not only for the active power filter control, but also for analysis and identification of power properties of three-phase systems with nonsinusoidal voltages and currents [42].

In this work the *pq* theory is used for the instantaneous power calculation without considering the neutral wire [28]. This theory consists of an algebraic transformation (Clarke transformation) of the three-phase voltages and currents in the *abc* coordinates to $\alpha\beta$. The equations for the current in the $\alpha\beta$ coordinates can be expressed as [28,43]:

$$\begin{bmatrix} i_\alpha \\ i_\beta \end{bmatrix} = \sqrt{\frac{2}{3}} \begin{bmatrix} 1 & -\frac{1}{2} & -\frac{1}{1} \\ 0 & \frac{\sqrt{3}}{2} & -\frac{\sqrt{3}}{2} \end{bmatrix} \begin{bmatrix} i_a \\ i_b \\ i_c \end{bmatrix} \tag{13}$$

The voltage in $\alpha\beta$ coordinates will be

$$\begin{bmatrix} v_\alpha \\ v_\beta \end{bmatrix} = \sqrt{\frac{2}{3}} \begin{bmatrix} 1 & -\frac{1}{2} & -\frac{1}{1} \\ 0 & \frac{\sqrt{3}}{2} & -\frac{\sqrt{3}}{2} \end{bmatrix} \begin{bmatrix} v_a \\ v_b \\ v_c \end{bmatrix} \tag{14}$$

The equation for p, q is

$$\begin{bmatrix} p \\ q \end{bmatrix} = \begin{bmatrix} v_\alpha & v_\beta \\ v_\beta & -v_\alpha \end{bmatrix} \begin{bmatrix} i_\alpha \\ i_\beta \end{bmatrix} \tag{15}$$

The complete system with the controller is shown in Fig. 7. In the first part of the controller, the instantaneous value of real and imaginary power are calculated and to generate the reference value of p and q, they pass through a selection block, where the power has been calculated which need to be compensated as shown in Fig. 8. Then the error current signal used to switch the inverter is available, as shown in Fig. 9.

The HVDC link converter behaves like a nonlinear load [44]. A nonlinear load draws a fundamental or average and a harmonic or oscillating current component from the power system. A shunt active filter can compensate both oscillating and average current [28]. The real and imaginary power can be defined as the combination of average and oscillating components. The undesirable oscillating real and reactive power are produced by the harmonics components in the load current. The compensating currents in $\alpha\beta$ reference can be calculated for this oscillating power. Then, the Clarke inverse transformation is used to calculate the amount of current to be injected by the virtual active filter. To generate the current for the controller, Eq. (15) can be written as

$$\begin{bmatrix} i_\alpha \\ i_\beta \end{bmatrix} = \frac{1}{v_\alpha^2 + v_\beta^2} \begin{bmatrix} v_\alpha & v_\beta \\ v_\beta & -v_\alpha \end{bmatrix} \begin{bmatrix} p \\ q \end{bmatrix} \tag{16}$$

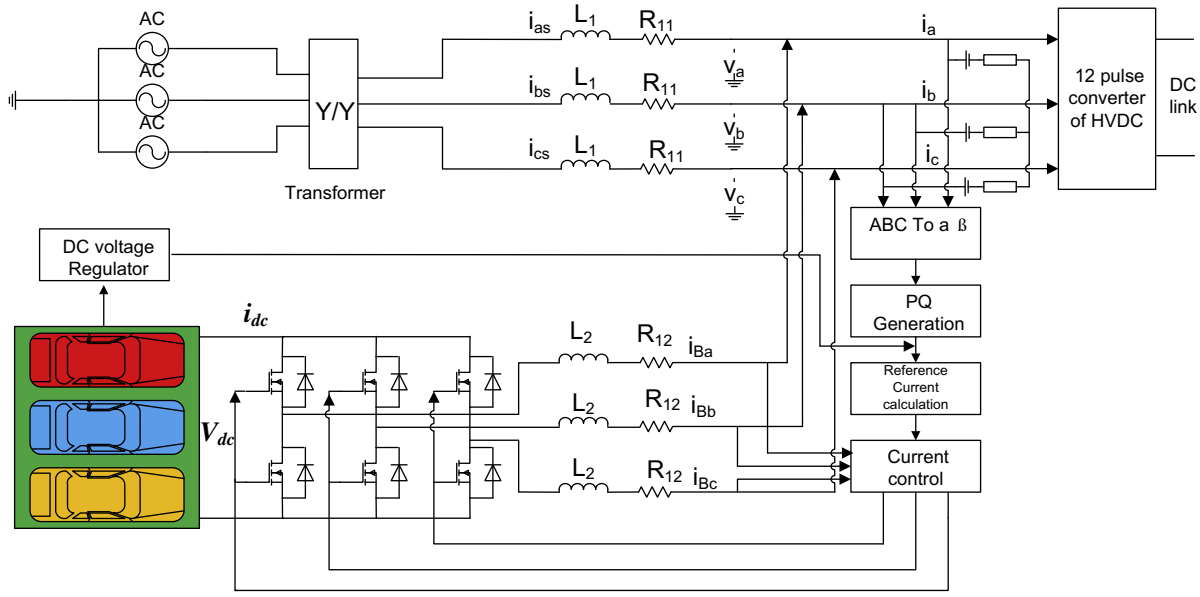

Fig. 7. PHEVs connection with HVDC network as virtual active filter.

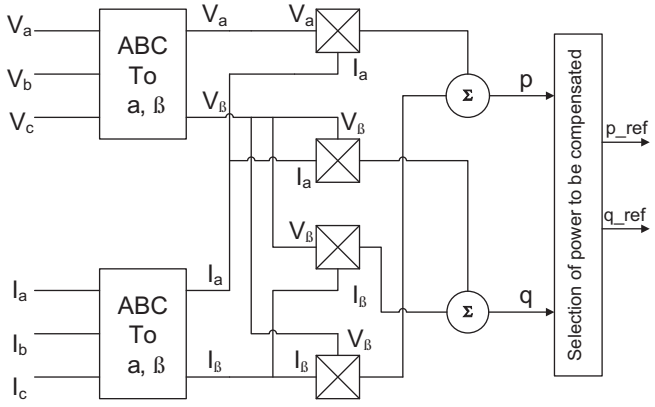

Fig. 8. *pq* generation in controller.

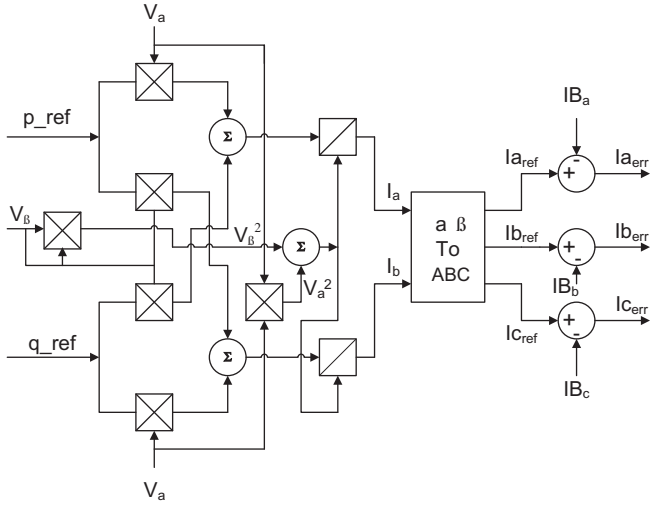

Fig. 9. Signal generation for inverter switching.

4.3. Power compensation section

It is convenient to separate p and q into their average and oscillating parts as

$$p = \bar{p} + \tilde{p} \tag{17}$$

$$q = \bar{q} + \tilde{q} \tag{18}$$

where $\bar{p}$ and $\tilde{p}$ are the average parts of real and imaginary power respectively, and $\bar{q}$ and $\tilde{q}$ are the oscillating parts of real and imaginary power respectively.

From Eq. (16), it is possible to write

$$\begin{bmatrix} i_\alpha \\ i_\beta \end{bmatrix} = \frac{1}{v_\alpha^2 + v_\beta^2}\begin{bmatrix} v_\alpha & v_\beta \\ v_\beta & -v_\alpha \end{bmatrix}\begin{bmatrix} p \\ 0 \end{bmatrix} + \frac{1}{v_\alpha^2 + v_\beta^2}\begin{bmatrix} v_\alpha & v_\beta \\ v_\beta & -v_\alpha \end{bmatrix}\begin{bmatrix} 0 \\ q \end{bmatrix} \tag{19}$$

$$\triangleq \begin{bmatrix} i_{\alpha p} \\ i_{\beta p} \end{bmatrix} + \begin{bmatrix} i_{\alpha q} \\ i_{\beta q} \end{bmatrix} \tag{20}$$

where the instantaneous active and reactive current in $\alpha\beta$ axis are denoted by $i_{\alpha p}$, $i_{\beta p}$ and $i_{\alpha q}$, $i_{\beta q}$ respectively. The reactive power is defined as a component of the instantaneous power, as shown in Eq. (21). The instantaneous power in the $\alpha\beta$ axis are p_α and p_β which are combinations of the instantaneous active and reactive power in the α axis ($p_{\alpha p}$ and $p_{\alpha q}$) and β axis ($p_{\beta p}$ and $p_{\beta q}$) respectively. In the p–q theory, the imaginary power means the sum of products of the instantaneous three phase voltages and currents. In this study q represents the imaginary power.

Therefore the instantaneous power (p) in the $\alpha\beta$ axis can be expressed as

$$\begin{aligned} p &= v_\alpha i_{\alpha p} + v_\beta i_{\beta p} + v_\alpha i_{\alpha q} + v_\beta i_{\beta q} \\ &= \frac{v_\alpha^2}{v_\alpha^2 + v_\beta^2}p + \frac{v_\beta^2}{v_\alpha^2 + v_\beta^2}p + \frac{v_\alpha v_\beta}{v_\alpha^2 + v_\beta^2}q + \frac{-v_\alpha v_\beta}{v_\alpha^2 + v_\beta^2}q \\ &= p_{\alpha p} + p_{\beta p} + p_{\alpha q} + p_{\beta q} = p_\alpha + p_\beta \end{aligned} \tag{21}$$

As the sum of the third and fourth terms on the right hand side in Eq. (21) is always zero, this is why they were named as instantaneous reactive power while the instantaneous imaginary power (q) is a quantity that gives the magnitudes of the power $p_{\alpha q}$ and $p_{\beta q}$. If the $\alpha\beta$ variables of the instantaneous real power (p) and

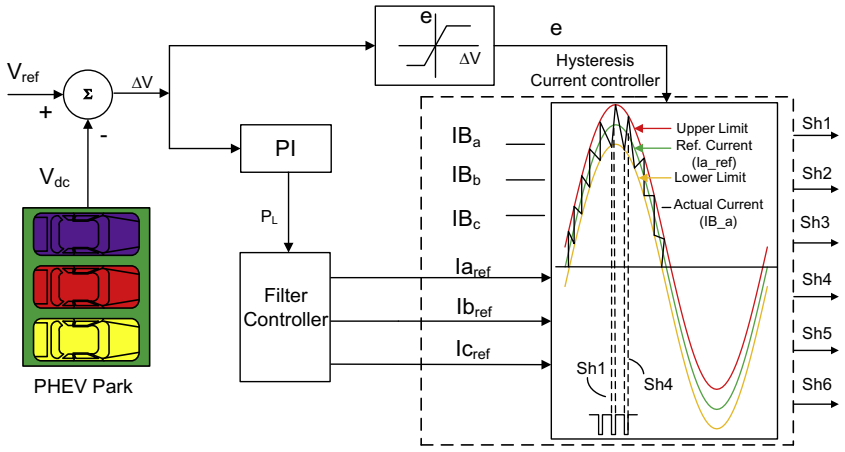

Fig. 10. Signal generation for inverter switching with hysteresis band.

imaginary power (q) defined in Eq. (15) are replaced by their equivalent expressions referred to the *abc* axis using Eq. (13) and similarly for the current, the following relationship can be found:

$$\begin{aligned} p &= v_\alpha i_\alpha + v_\beta i_\beta \\ &= \frac{1}{3}[\{(v_a - v_b) - (v_c - v_a)\}i_a + \{(v_b - v_c) - (v_a - v_b)\}i_b \\ &\quad + \{(v_c - v_a) - (v_b - v_c)\}i_c] \\ &= \frac{1}{3}[(v_{ab} - v_{ca})i_a + (v_{bc} - v_{ab})i_b + (v_{ca} - v_{bc})i_c] \end{aligned} \tag{22}$$

and

$$\begin{aligned} q &= v_\beta i_\alpha + v_\alpha i_\beta = \frac{1}{\sqrt{3}}[(v_a - v_b)i_c + (v_b - v_c)i_a + (v_c - v_a)i_b] \\ &= \frac{1}{\sqrt{3}}(v_{ab}i_c + v_{bc}i_a + v_{ca}i_b) \end{aligned} \tag{23}$$

In order to draw a constant instantaneous power from the source, the shunt virtual active filter should be installed as close as possible to the nonlinear load. In this case we have considered that the average real power $\bar{p}$ will be supplied by the grid. The power P_L from the voltage regulator contributes to maintaining V_{dc} around their reference value (300 V). In fact, a small amount of average real power P_L, must be drawn continuously to supply switching and Ohmic losses in the converters. The oscillating real power $\tilde{p}$, the power P_L and the total instantaneous reactive power ($q = \bar{q} + \tilde{q}$) will be compensated by the virtual filter. Therefore the compensating current will be

$$\begin{bmatrix} i_{com\alpha} \\ i_{com\beta} \end{bmatrix} = \frac{1}{v_\alpha^2 + v_\beta^2}\begin{bmatrix} v_\alpha & v_\beta \\ v_\beta & -v_\alpha \end{bmatrix}\begin{bmatrix} -\tilde{p} + P_L \\ -q \end{bmatrix} \tag{24}$$

where $\tilde{p}$ can be calculated using $p = \tilde{p}$ in Eqs. (19) and (20). The use of a PHEV park as a source of energy has the advantage of compensating the real power (p) which implies an oscillating flow of energy, protect from experiencing large voltage variations. If the amplitude of the AC voltage is higher than the DC voltage the PWM controller loses its controllability, in this case the rating of DC capacitor need to be large. However using a PHEV park as storage this problem can be eliminated.

4.4. DC voltage regulator and current controller

In this paper the hysteresis current controller is used because it offers excellent dynamic performance and also very simple to implement in real time [45]. A dynamic offset (ε) is created from the measurement of V_{dc} and the DC reference voltage in such way that the band limits of the hysteresis current controller will be:

$$\text{Upper hysteresis band limit} = i_{(ref)} + \Delta(1 + \epsilon)$$

$$\text{Lower hysteresis band limit} = i_{(ref)} - \Delta(1 + \epsilon)$$

where $i_{ref} = ia_{ref}$, ib_{ref}, ic_{ref} and Δ is a fixed half hysteresis band. Another slower feedback loop generates the power P_L from the voltage regulator to keep the voltage around a fixed reference point, as shown in Fig. 10. It brings the energy balance and also useful for compensating the error which occur during the transient state.

The switching logic for the hysteresis current controller is formulated as:

- if $iB_a < (ia_{ref} - \Delta(1 + \varepsilon))$ Sh 1 on and Sh 4 off
- if $iB_a < (ia_{ref} + \Delta(1 + \varepsilon))$ Sh 1 off and Sh 4 on
- if $iB_b < (ib_{ref} - \Delta(1 + \varepsilon))$ Sh 3 on and Sh 6 off
- if $iB_b < (ib_{ref} + \Delta(1 + \varepsilon))$ Sh 3 off and Sh 6 on
- if $iB_c < (ic_{ref} - \Delta(1 + \varepsilon))$ Sh 5 on and Sh 2 off
- if $iB_c < (ic_{ref} + \Delta(1 + \varepsilon))$ Sh 5 off and Sh 2 on

5. Simulation results

The 12 pulse converter of an HVDC network is a major source of harmonics in power systems. In order to realize the performance of virtual active filter two different case studies are introduced:

1. A virtual active filter on the rectifier side, and
2. A virtual active filter on each of the rectifier and inverter sides.

5.1. Case1: virtual filter on rectifier side

In this study, a virtual active filter is connected on the rectifier side and a fixed tuned filter on the inverter side. Three different analyses have been carried out to identify the performances of the virtual active filter in the HVDC link. A real time harmonics current spectrum is analyzed and it is determined that its different orders have the maximum and minimum levels of 0.21% and 0.01% magnitude respectively as shown in Fig. 11. These harmonic currents are periodic at a period twice of the system frequency for p–q theory [28]. The THDs of the current for the virtual filter are also investigated and found to be 4.16% for the transient condition and 0.3% for the steady state as shown in Fig. 12. According to IEEE standard 519 [46], these THD levels for current are within the acceptable limits. To recognize the individual harmonics spectra another analysis is carried out. As a 12 pulse converter does not

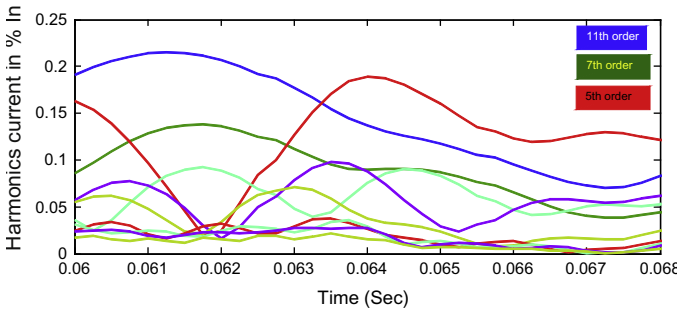

Fig. 11. Harmonics currents of load (one cycle) with virtual filter (case1).

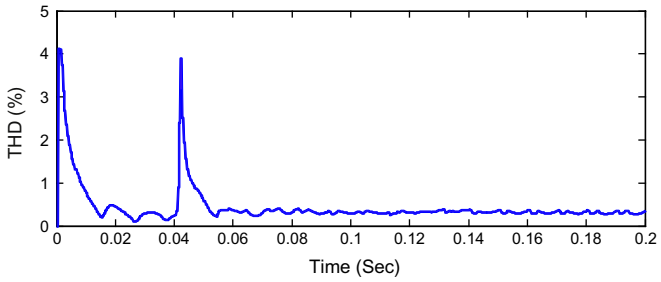

Fig. 12. THD with virtual filter (case1).

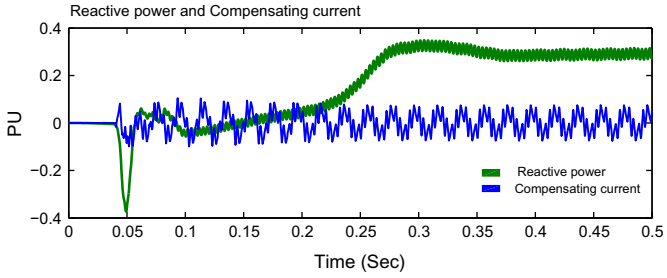

Fig. 13. Compensating current and reactive power outputs from virtual filter.

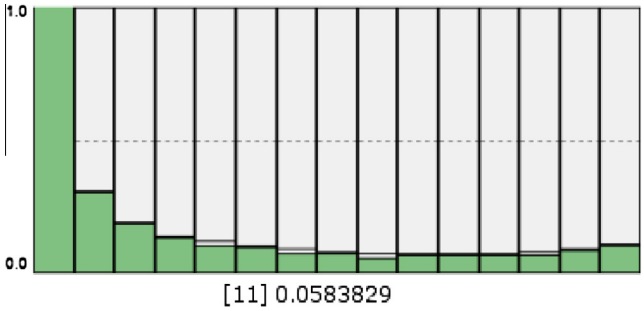

Fig. 14. Harmonics spectrum of source current with virtual filter.

produce significant 5th and 7th order harmonics and the major contributor is 11th order harmonics [47], therefore 11th order harmonics magnitude are observed for both the source and load current using virtual filter as shown in Figs. 14 and 15 respectively and are 0.058% and 0.011% respectively. To realize the characteristics of the compensating current and instantaneous reactive power the wave form is shown in Fig. 13 in which the PHEV park's capability to filter is justified.

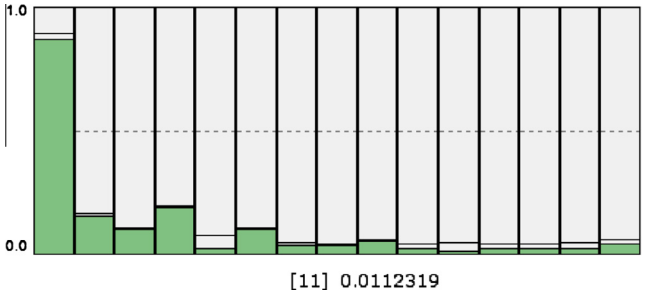

Fig. 15. Harmonics spectrum of load current with virtual filter.

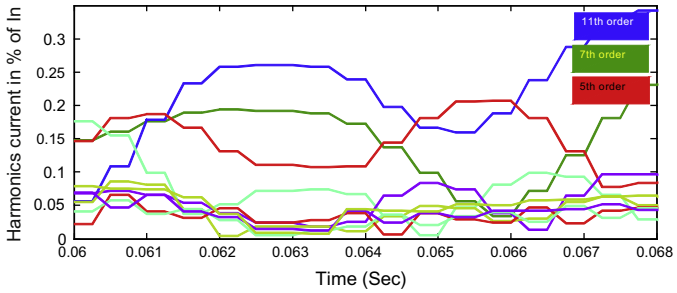

Fig. 16. Harmonics currents of inverter side (one cycle) with virtual filter (case2).

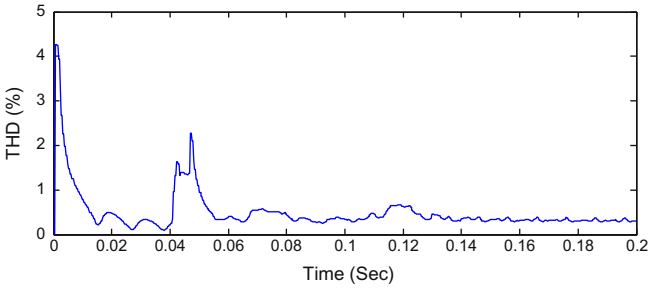

Fig. 17. THD with virtual filter (case2).

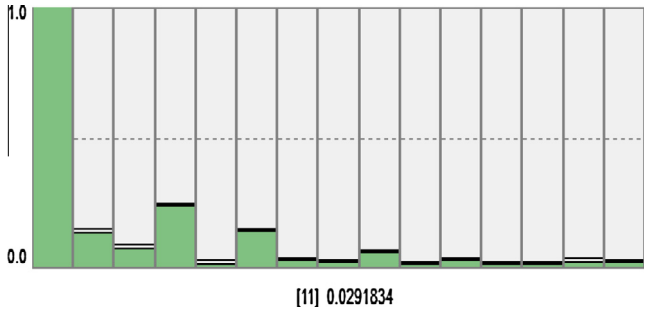

Fig. 18. Harmonics spectrum of load current with virtual filter (case2).

5.2. Case2: virtual filter on both converter side

To justify the performance of the PHEV base virtual filter, virtual active filters are used at both sides of the HVDC link and, in these analyses; all the simulation results are taken from the inverter side. To determine this virtual active filter's real-time harmonics current spectrum, Fig. 16 shows it has a maximum harmonics current level of 0.32% and a minimum of 0.013%. The THDs of its currents are 4.3% for the transient condition and 4% for the steady

state, as shown in Fig. 17. An individual spectrum analysis of the virtual active filter's harmonics load currents also shows that the magnitude of its 11th order harmonics current is 0.02918, as shown in Fig. 18. These analyses show that, as the performances of the virtual active filter can satisfy the requirements of IEEE Std 519-1992, it could be used as an economical solution for the HVDC link.

6. Conclusions

The goal achieved through this study is the successful demonstration of the filtering and reactive power compensation using PHEVs as active filters in an HVDC network. We investigated the converters and system harmonics currents using a virtual active filter in the system for two different cases. The simulation results obtained showed that the harmonics reduction performance of an HVDC network with PHEV used as an active filter is within the acceptable range. The implementation of PHEVs as virtual active filters in HVDC networks provide the opportunities to use active filter in a cost effective way and ensure connecting points of a PHEV park at HVDC converter terminals. It has been concluded that the application of the bidirectional converters of PHEVs of a PHEV park in a power system offers great opportunities for the future but also number of challenges. A great deal of research into the implementation of V2G technology in an HVDC network is essential. Several issues, such as using a better control technique and PHEVs as a source, could be interesting topics for future work.

Appendix A

A.1. Battery parameters

The parameters used for the Battery are as follows:
Parameters referring to the battery capacity:

$$I^* = 49\ \text{A},\ K_p = 1.18,\ C_1 = 261.9\ \text{A h},\ \theta_f = -40\ ^\circ\text{C}$$

Parameters referring to the main branch of the electric equivalent:

$$T_s = 28,800\ \text{s},\ E_{m0} = 2.135\ \text{V},\ K_e = 0.580\ \text{e}^{-3}\ \text{V}/^\circ\text{C},$$
$$A_0 = -0.30,\ R_{00} = 2.0\ \text{m}\,\Omega,\ R_{10} = 0.4\ \text{m}\,\Omega$$

Parameters referring to the parasitic reaction branch:

$$V_{po} = 0.1\ \text{V},\ A_p = 2.0,\ G_{po} = 2pS$$

Parameters referring to the battery thermal model:

$$C_\theta = 15\ \text{Wh}/^\circ\text{C},\ R_\theta = 0.2\ ^\circ\text{C/W}$$

References

[1] Lemoine DM, Kammen DM, Farrell AE. An innovation and policy agenda for commercially competitive plug in hybrid electric vehicles. Environ Res Lett 2008;3(1):014003.
[2] Sovacool Benjamin K, Hirsh Richard F. Beyond batteries: an examination of the benefits and barriers to plug in hybrid electric vehicles (PHEVs) and a vehicle to grid (V2G) transition. Energy Policy 2009;37(3):095–1103.
[3] Das T, Aliprantis D. Small signal stability analysis of power system integrated with PHEVs. In: Energy 2030 conference, energy 2008 IEEE; 2008. p. 1–4.
[4] Kobayashi Y, Kiyama N, Aoshima H, Kashiyama M, A route search method for electric vehicles in consideration of range and locations of charging stations. In: Intelligent vehicles symposium (IV), IEEE; 2011. p. 920–5.
[5] Meng W, Kai L. Optimization of electric vehicle charging station location based on game theory. In: International conference on transportation, mechanical, and electrical engineering (TMEE); 2011. p. 809–812.
[6] Preetham G, Shireen W. Photovoltaic charging station for plug in hybrid electric vehicles in a smart grid environment. In: Innovative smart grid technologies (ISGT), IEEE PES; 2012. p. 1–8.
[7] Jia L, Hu Z, Song Y, Luo Z. Optimal sitting and sizing of electric vehicle charging stations. In: Electric vehicle conference (IEVC); 2012. p. 1–6.
[8] Moradijoz M, Moghaddam MP, Haghifam M, Alishahi E. A multiobjective optimization problem for allocating parking lots in a distribution network. Int J Electr Power Energy Syst 2013;46:115–22.
[9] Kempton W, Tomic J. Vehicle to grid power fundamentals: calculating capacity and net revenue. J Power Sources 2005;144:268–79.
[10] Guille C, Gross G. A conceptual framework for the vehicle to grid V2G implementation. Energy Policy 2009;37(11):4379–90.
[11] Kempton W, Tomić J. Vehicletogrid power implementation: from stabilizing the grid to supporting large scale renewable energy. J Power Sources 2005;144(1):280–94.
[12] Islam FR, Pota HR. V2G technology to improve wind power quality and stability. In: Australian control conference (AUCC); 2011. p. 452–457.
[13] Mitra P, Venayagamoorthy G, Corzine K. Smart Park as a virtual STATCOM. In: IEEE trans on smart grid 2011;2(3):445–455.
[14] Islam FR, Pota HR. Plug in hybrid electric vehicles park as virtual DVR. Electron Lett 2013;49(3):211–3.
[15] Islam FR, Pota HR. PHEVs park as virtual UPFC. TELKOMNIKA Indones J Electr Eng 2012;10(8):2285–94.
[16] Hutson C, Venayagamoorthy G, Corzine K. Intelligent scheduling of hybrid and electric vehicle storage capacity in a parking lot for profit maximization in grid power transactions. In: Energy 2030 conference, energy 2008 IEEE; 2008. p. 1–8.
[17] Saber AY, Venayagamoorthy GK. Intelligent unit commitment with vehicle to grid a costemission optimization. J Power Sources 2012;195(3):898–911.
[18] Gunnarsson Stefan, Jiang L, Petersson Anders. Active filters in HVDC transmission.http://www.abb.com/hvdc
[19] Rodger JA. Toward reducing failure risk in an integrated vehicle health maintenance system: A fuzzy multisensor data fusion Kalman filter approach for IVHMS. Expert Syst Appl 2012;39(10):9821–36.
[20] Islam FR, Pota HR. Design a PVAF system using V2G technology to improve power quality. In: 37th annual conference on IEEE industrial electronics society, (IECON 2011), November 2011. p. 861–6.
[21] Islam FR, Pota HR, Ali MS. V2G technology for designing active filter system to improve wind power quality. In: 21st Australasian Universities Power Engineering Conference (AUPEC 2011); 2011. p. 1–6.
[22] Laughton MA, Warne D, editors. Electrical engineer's reference book. Elsevier; 2003.
[23] IEEE guide for the evaluation of the reliability of HVDC converter stations, IEEE Std 1240-2000; 2001. http://dx.doi.org/10.1109/IEEESTD.2001.245621.
[24] Agelidis V, Demetriades G, Flourentzou N. Recent advances in high voltage directcurrent power transmission systems. In: IEEE international conference on industrial technology; 2006. p. 206–13.
[25] Flourentzou N, Agelidis V, Demetriades G. VSC based HVDC power transmission systems: an overview. IEEE Trans Power Electr 2009;24(3):592–602.
[26] Zhang X, Bai J, Cao G, Chen C. Optimizing HVDC control parameters in multiinfeed HVDC system based on electromagnetic transient analysis. Int J Electr Power Energy Syst 2013;49:449–54.
[27] Kili U, Ayan K. Optimizing power flow of AC–DC power systems using artificial bee colony algorithm. Int J Electr Power Energy Syst 2013;53:592–602.
[28] Akagi H, Watanabe E, Aredes M. Instantaneous power theory and applications to power conditioning. Willey Interscience; 2007.
[29] Peng FZ, Lai JS. Generalized instantaneous reactive power theory for threephase power systems. IEEE Trans Instrum Measur 1996;45(1):592–602.
[30] Mikkili S, Panda A. Real time implementation of PI and fuzzy logic controllers based shunt active filter control strategies for power quality improvement. Int J Electr Power Energy Syst 2012;43(1):1114–26.
[31] Kimbark EW. Direct current transmission. WilleyInterscience; 1971.
[32] Ainsworth JD. Proposed benchmark model for study of HVDC controls by simulator or digital computer. In: Proc CIGRE SC14 Colloquium on HVDC with weak AC systems, Maidstone, UK, September 1985
[33] Szechtman M, Wess T, Thio C. A benchmark model for HVDC system studies. In: International conference on AC and DC power transmission, September 1991. p. 374–8.
[34] Faruque M, Zhang Y, Dinavahi V. Detailed modeling of CIGRE HVDC benchmark system using PSCADEMTDC and PSBSIMULINK. IEEE Trans Power Del 2006;21(1):378–87.
[35] Kisacikoglu M, Ozpineci B, Tolbert L. Examination of a PHEV bidirectional charger system for V2G reactive power compensation. In: Applied power electronics conference and exposition (APEC21); 2010. p. 458–65.
[36] Saft hybrid electric military vehicle data sheet. <http://www.saftbatteries.com/doc/Documents/defence/Cube769/HEMV%205-8%20Data%20Sheet.74ee69b4-34ed-49b5-a870-bd5f6160ab8d.pdf>.
[37] Ceraolo M. New dynamical models of lead-acid batteries. IEEE Trans Power Syst 2000;15(4):1184–90.
[38] Barsali S, Ceraolo M. Dynamical models of lead-acid batteries: implementation issues. IEEE Trans Energy Convers 2002;17(1):16–23.
[39] Milano F. Power system modelling and scripting. New York: Springer-Verlag; 2010.
[40] Tremblay O, Dessaint LA, Dekkiche AI. A generic battery model for the dynamic simulation of hybrid electric vehicles. In: Vehicle power and propulsion conference; 2007. p. 284–9.
[41] Crosier RSWYC. Modelling of a grid connected, multifunctional electric vehicle charging station in active filter mode with *dq* theory. In: Energy conversion congress and exposition (ECCE 2012); 2012. p. 3395–402.
[42] Czarnecki LS. Instantaneous reactive power pq theory and power properties of threephase systems. IEEE Trans Power Del 2006;21(1):362–7.

[43] Watanabe EH, Aredes M, Akagi H. The p–q theory for active filter control: some problems and solutions. Trans Revista Control Autom 2004;15(1).
[44] Singh A, Singh B. Performance evaluation of power converters with distribution static compensator. In: Joint international conference on power electronics, drives and energy systems (PEDES 2010) India; 2010. p. 1–5
[45] Tilli A, Tonielli A. Sequential design of hysteresis current controller for threephase inverter. IEEE Trans Ind Electr 1998;45(5):771–81.
[46] IEEE Std 519-1992, IEEE Recommended Practices and Requirements for Harmonic Control in Electric Power Systems© Institute of Electrical and Electronics Engineers, Inc.; 1993.
[47] Cheng Po-Tai, Bhattacharya S, Divan D. Application of dominant harmonic active filter system with 12 pulse nonlinear loads. IEEE Trans Power Del 1999;14(2):642–7.